Nano Energy 135 (2025) 110656

Contents lists available at ScienceDirect

Nano Energy

journal homepage: www.elsevier.com/locate/nanoen

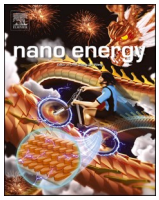

Integrated triboelectric self-powering and piezoresistive self-sensing cementitious composites for intelligent civil infrastructure

Wenkui Dong [a], Shuhua Peng [b,*], Kejin Wang [c], Yuhan Huang [d], Long Shi [e], Fan Wu [d], Wengui Li [a,*]

[a] Centre for Infrastructure Engineering and Safety, School of Civil and Environmental Engineering, The University of New South Wales, NSW 2052, Australia
[b] School of Mechanical and Manufacturing Engineering, The University of New South Wales, NSW 2052, Australia
[c] Department of Civil, Construction, and Environmental Engineering, Iowa State University, IA 50011, USA
[d] School of Civil and Environmental Engineering, University of Technology Sydney, NSW 2007, Australia
[e] State Key Laboratory of Fire Science, University of Science and Technology of China, Hefei 230026, China

ARTICLE INFO

Keywords:
Cement-based triboelectric nanogenerator (CBTENG)
Cement-based sensor
Nano carbon black
Triboelectrification
Piezoresistivity
Surface condition

ABSTRACT

Self-powering and self-sensing concrete materials are critical for advancing intelligent civil infrastructure, particularly in powering various sensors used in structural health monitoring (SHM). This study developed an integrated cement-based triboelectric nanogenerator (TENG) and piezoresistive self-sensing sensors using fully cured nano carbon black (NCB)-reinforced cement mortar. In the cement-based TENG (CBTENG), a thin cement plate served as the positive triboelectric layers, while a polytetrafluoroethylene (PTFE) plate served as the negative triboelectric layers. The electrical output voltage increased with both the loading frequency and surface contact area. At a frequency of 4.0 Hz, the 40 mm × 40 mm × 5 mm CBTENG generated a short-circuit current of 8.2 μA and an open-circuit voltage of up to 113 V. This output was sufficient to recharge a 10 μF capacitor to 0.32 V within 25 seconds after rectification. A comparison of the triboelectric performance of CBTENGs with different surface areas revealed that larger specimens had a lower percentage of effective contact area. This was attributed to the uneven surfaces of both the cement-based and PTFE plates, as well as small protrusions and holes on the cement-based surface. The piezoresistive cement-based sensors demonstrated excellent self-sensing capabilities under various loading amplitudes, rates, and conditions, including both compression and bending. These sensors performed effectively whether used independently or embedded inside concrete beams. These findings pave the way for self-powering and self-sensing structure systems, leveraging triboelectric and piezoresistive effects to power sensors in smart civil infrastructure and SHM applications.

1. Introduction

Civil infrastructure is frequently subjected to external mechanical loadings such as those from vehicles, pedestrians, vibrations, wind, water flow, ocean waves, etc. These mechanical loadings often cause structural cracks and even failure. Hence, it is necessary to propose novel methods for the structural health monitoring (SHM) of civil infrastructures. The cement-based sensor is created by incorporating conductive fillers into widely used cementitious materials, transforming them into sensors with piezoresistive properties [1–4]. This sensor monitors the external loads applied to the cement matrix by detecting changes in conductivity, which result from the relative movement of the conductive fillers within the matrix [5–8]. In addition to the monitoring of these mechanical loadings, if solutions could be employed to mitigate and harness the mechanical energy, it would not only protect the infrastructure but also have the chance to efficiently utilize the applied mechanical energy. Triboelectric nanogenerators (TENGs), which convert mechanical energy into electrical energy through the triboelectric effect and electrostatic induction, represent an innovative energy harvesting technology [9–12]. Integrating cement-based sensors and TENG technology with civil infrastructure holds the potential to capture the mechanical energy applied to these infrastructures and convert it into electrical energy for powering cement-based sensors. This approach could significantly reduce the electrical energy required for infrastructure operation, thereby contributing to the goals of carbon emission reduction and sustainable development in civil engineering.

* Corresponding authors.
E-mail addresses: shuhua.peng@unsw.edu.au (S. Peng), wengui.li@unsw.edu.au (W. Li).

https://doi.org/10.1016/j.nanoen.2025.110656
Received 4 November 2024; Received in revised form 6 January 2025; Accepted 6 January 2025
Available online 9 January 2025

Cement-based sensors have emerged as promising technology in the field of SHM. These sensors are designed to be integrated directly into concrete structures, allowing for real-time monitoring of stress, strain, and damage. Early research focused on embedding conductive materials, such as carbon fibers or steel fibers, into the cement matrix to create a piezoresistive effect, where changes in electrical resistance correspond to mechanical stresses [13–16]. Through the years, developments in nanotechnology have further enhanced the sensitivity and accuracy of these sensors, leading to the incorporation of nanomaterials like graphene, carbon nanotubes, and nano carbon black (NCB) in cement-based sensors [17–21]. However, like other sensors, cement-based sensors require an external power supply to monitor the electrical conductivity of the cement matrix.

The concept of TENG was first introduced in 2012, when researchers sought to develop a sustainable and efficient method for harvesting ambient mechanical energy from sources such as human motion, vibrations, and environmental forces [22–24]. The ability of two objects to generate charges through friction is influenced by various factors, including the surface properties, environmental conditions, dielectric properties, and electrical conductivity of the materials. Nanomaterials with high surface energy facilitate charge transfer, thereby increasing the generation of triboelectric charges. Studies have found that the incorporation of nano TiO_2 [25] or NCB [26] into TENG can enhance surface energy greatly. Additionally, increased surface roughness enlarges the actual contact area of triboelectric layers, which boosts the generation of triboelectric charges. Hence, a material with a high dielectric constant and low electrical conductivity can enhance triboelectric efficiency.

Cement-based TENG (CBTENG) can be applied in buildings, roads, bridges, and other infrastructure to enable large-scale mechanical energy harvesting and utilization. Compared to traditional triboelectric materials, cement-based materials offer advantages such as high strength, low cost, abundant resources, and high durability. There has been limited research on using cement-based materials as positive triboelectric material, and the findings showed that the modified cement-based TENG with TiO_2 can generate a much higher voltage of 102.8 V and power density of 265 mW/m^2 compared to other materials such as glass, nylon, aluminum, and copper [27]. The addition of rubber into cementitious materials can alter the electrical conductivity and dielectric properties [28–30]. Despite the reduction in dielectric constant, rubber modified cement-based TENG can still enhance triboelectric performance, attributed to the increased surface area and friction coefficient provided by the rubber particles [31]. With a proper dosage of 0.04 wt% NCB, the nanoengineered cement paste has been demonstrated with excellent triboelectric properties, whose voltage and power density can reach 110 V and 2.13 W/m^2, respectively [32]. However, the studies on CBTENG used cementitious materials cured for 7 days, which does not reflect the actual conditions of concrete applications. Although Dong et al. [33] achieved the fully cured CBTENG with a short-circuit current and open-circuit voltage peaking at 3.62 μA and 279.4 V, the cement materials with real-world characteristics are more required to fully understand their sensing and energy harvesting performance in civil infrastructures.

To address this gap, this work employs cement-based materials that closely mirror those used in real civil infrastructure, investigating the performance of fully cured CBTENG. Nano carbon black (NCB) was incorporated into the cement matrix to enhance their dielectric and conductive properties, thereby improving their performance as tribopositive materials when paired with polytetrafluoroethylene (PTFE) as the tribonegative layer for TENGs [48,49]. In addition, the piezoresistive self-sensing performances of NCB filled cement-based sensors were also investigated when subjected to various loadings. In terms of triboelectric self-powering performance, it was found that the output voltage increases with loading frequency. Additionally, small protrusions and holes present on the cement-based surface contribute to an increased surface contact area, enhancing the output of TENG. For piezoresistive self-sensing characteristics, the electrical resistance changes of cement-based sensors correlate well to the applied forces whether in direct loading conditions or in embedded applications. This study aims to explore the feasibility of integrating self-powering and self-sensing capabilities into civil infrastructure through innovative NCB filled cementitious materials. Our goal is to provide new insights and advancements for the development of future smart cities, contributing to more sustainable and technologically advanced urban environments [50,51].

2. Experimental details

2.1. Chemicals and materials

Portland cement with a 10 % replacement ratio by silica fume is the binder material. The addition of extremely fine silica fumes can fill the micro-voids in the cement matrix to enhance the density and mechanical strengths. The commercial river sand was used as fine aggregate, with a well-graded particle size from 75 μm to 4.75 mm and a sand-to-binder ratio of 2.0. NCB produced from Xinxiang Deron Chemical Co, Ltd, China is used to ameliorate the dielectric and conductive properties of cement matrix, and its physical and chemical properties are listed in Table 1. The high-range water reducer purchased from SIKA Australia Co., Ltd. has been applied to assist NCB dispersion and improve the workability of the cement matrix. The amount used is 0.8 % by weight of binder. Deionized water is used to mix the cementitious materials. Additionally, other materials for installing the CBTENG include the insulated acrylic substrate, elastic foam, nickel foam electrode, epoxy adhesive, conductive glue, and another triboelectric polytetrafluoroethylene (PTFE) layer. The PTFE plate is purchased from the PURESHI Co., Ltd, China; the elastic foam is obtained from the SHOWJIE Co., Ltd, China and the nickel foam is from the Kunshan Bozuan New Material Co., Ltd, China. The epoxy adhesive is purchased from Selleys Co., Ltd, Australia. The PTFE is selected as a negative triboelectric layer due to its excellent electron affinity. The physical and chemical properties of PTFE are listed in Table 2. Since highly conductive materials tend to facilitate charge transfer during friction and lead to rapid charge neutralization, it prevents the accumulation of triboelectric charges and reduces triboelectric efficiency. Therefore, the NCB content must be within the percolation threshold in cementitious materials. Based on the previous studies, the dosage of 0.5 % NCB is appropriate to improve the relative dielectric constant of cementitious materials without enhancing their electrical conductivity significantly [29].

2.2. Production of cement matrix and cement-based sensor

The fabrication of cement-based sensors has been introduced in the authors' previous studies, as illustrated in Fig. 1. The first step is the preparation of NCB Suspension. The NCB is prepared and dispersed in a water reducer solution. The purpose of this step is to achieve a uniform and stable suspension, which is crucial for ensuring consistent distribution of NCB within the cement matrix. The dispersion of NCB was achieved through a combination of mechanical stirring and chemical dispersion methods. Initially, prepare the aqueous solution required for the cement-based mortar production and add an appropriate amount of water reducing agent. In addition to improving the workability of the slurry, the water reducing agent also aids in dispersing the NCB [34]. Add the NCB to the solution while stirring mechanically for 5 minutes to

Table 1
Physical and chemical properties of nano carbon black.

Particle size (nm)	Resistivity (Ω·cm)	Pour density (g/l)	DBP (ml/100 g)	Surface area (m^2/g)	pH	Ash content (%)
20	< 0.43	0.375	280	254	7.5	< 0.3

Table 2
Physical and chemical properties of PTFE plate.

Specific gravity (g/cm^3)	Dynamic friction coefficient (g/l)	Thickness (mm)	Service temperature (°C)	Elongation (%)	Compressive strength (MPa)	Flexural strength (MPa)
2.2	0.06	2	−200–260	150–400	12	13.7–34.3

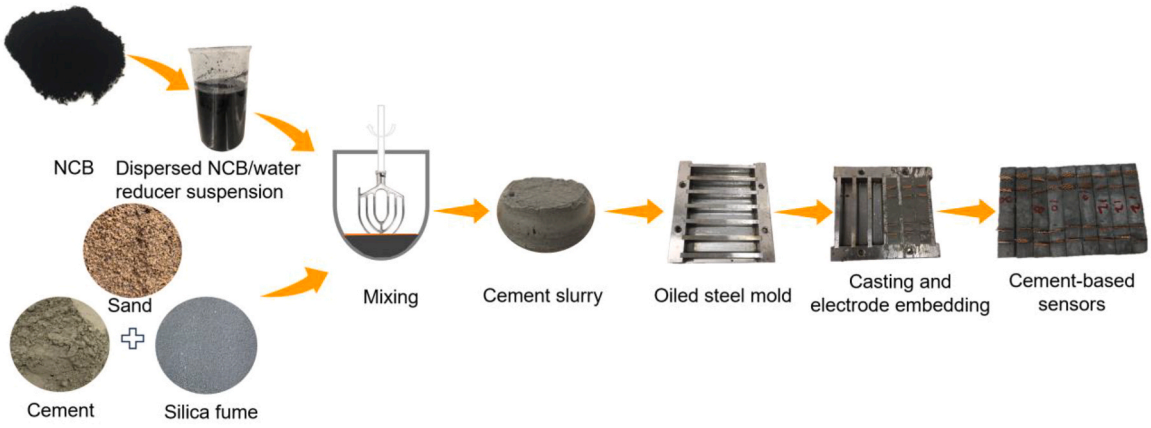

Fig. 1. Fabrication procedures of NCB filled cement-based sensors.

ensure no visible NCB agglomerates and air bubbles. Subsequently, insert an ultrasonic probe into the solution to further disperse the NCB suspension using ultrasonication for 30 minutes. The second step is to mix cementitious materials of cement and silica fume with NCB suspension. The cement, 10 % silica fume and sand mixture have been pre-mixed before being added to the dispersed NCB suspension. The cement acts as the primary binder, while the silica fume serves as a supplementary cementitious material, enhancing the overall performance of the cementitious composite. The mixing process is carried out thoroughly to ensure that the NCB is evenly distributed within the cementitious matrix, resulting in a homogenous cement slurry, as detailed in [35,36]. The homogenous cement slurry is then poured into pre-oiled steel molds. The oiling of the molds is an essential step to facilitate easy demolding, and to avoid any adhesion of the cement slurry to the mold surfaces. During the casting process, copper electrodes are embedded into the cement slurry. These electrodes are critical components that allow the resulting cementitious composite to function as a sensor by enabling the measurement of its electrical properties. After the cement slurry is poured into the molds and the electrodes are embedded, the mixture is allowed to be cured in a standard curing chamber at 23 ± 2 °C and humidity of 95 % until 28 days, forming solid cement-based sensors. These sensors are then demolded and undergo further processing or testing as needed.

2.3. Fabrication of CBTENG

Before fabricating CBTENG, it is necessary to cut the hardened cementitious specimens to specified dimensions. This study investigates the cement-based triboelectric layers at the sizes of 10 × 10 × 5 mm, 20 × 20 × 5 mm, 40 × 40 × 5 mm. To ensure optimal adhesive performance, the surfaces of acrylic substrate, cement mortar, and PTFE were thoroughly cleaned. Subsequently, the cement mortar, PTFE, and elastic foam were glued to the acrylic substrate, respectively. The glued components were left undisturbed at room temperature for at least half an hour. It is of significance to maintain the surface smoothness of the PTFE and acrylic substrate during this process to prevent any reduction in triboelectric effect caused by surface curvature. Additionally, the elastic foam was parallel to each other and perpendicular to the acrylic substrate to prevent instability and potential buckling damage during repeated loading. The abovementioned glue was a traditional epoxy adhesive, but the nickel foam working as electrodes of the cement-based layer was glued by the conductive adhesive, to eliminate the contact resistance between nickel foam and cement matrix. The components and final product of CBTENG can be found in Fig. 2.

2.4. Characterizations

All the tests are conducted for the fully cured cementitious materials after 28 days of curing. The compressive strength measurement is conducted on the cubic cementitious materials by a compression machine, along with a strain gauge attached to measure the deformation and compressive strain. Three duplicates are measured to obtain the average strength and deformation. The micromorphology of the cement matrix is observed by scanning electron microscope (SEM).

The CBTENG is designed to operate with a single electrode under a vertical contact-separation mode. It includes a bottom cement-based triboelectric layer and a top triboelectric PTFE layer. As shown in Fig. 3a, the experimental setup for the triboelectric self-powering test consists of several key components: a linear motor, a moving bed, a force cell, a current preamplifier, an oscilloscope, and a laptop for data acquisition. The moving bed, driven by the linear motor (Zaber LSQ450B-T3A), facilitates the relative motion between the cement plate and the PTFE plate. The current preamplifier collects the electrical signals generated by the triboelectric effect during the interaction between the cement and PTFE plates. The oscilloscope records the voltage output, which is displayed in real-time on the laptop screen. The maximum amplitudes of voltage and current, rather than their peak-to-peak values are collected as final results, as they represent the highest achievable energy output of CBTENG. A constant impact load of 10 N at varying frequencies from 1/2–4 Hz was applied in the triboelectric performance tests. All the tests are carried out in the environment with a temperature of 25 °C and relative humidity of 50 %.

As shown in Fig. 3b, the experimental setup for testing the piezoresistive self-sensing capabilities of the cement-based sensor involves a compression machine, a power supply, a resistor, multimeters, and the cement-based sensor with embedded electrodes. Electrical resistance is measured by direct current (DC) after the polarization gradually weakens. The cement-based sensor is connected to a circuit that includes a resistor and is monitored by multimeters to measure the change in electrical resistance under different loading conditions. The self-sensing

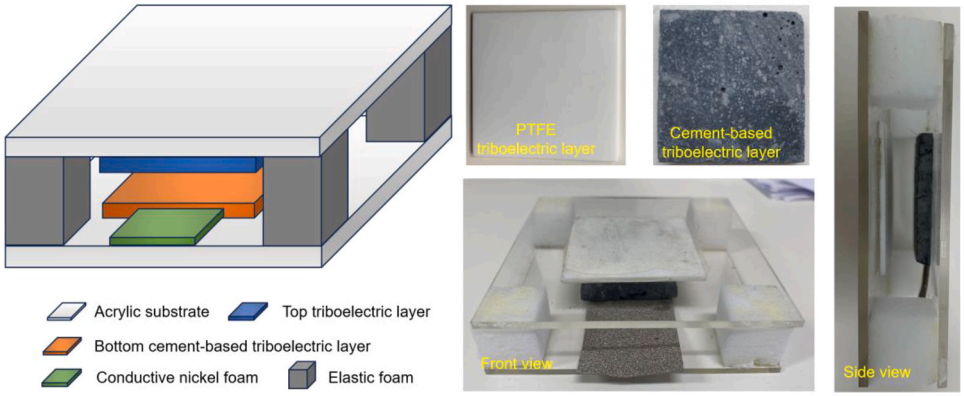

Fig. 2. Components, configuration and final product of self-powering cement-based TENG.

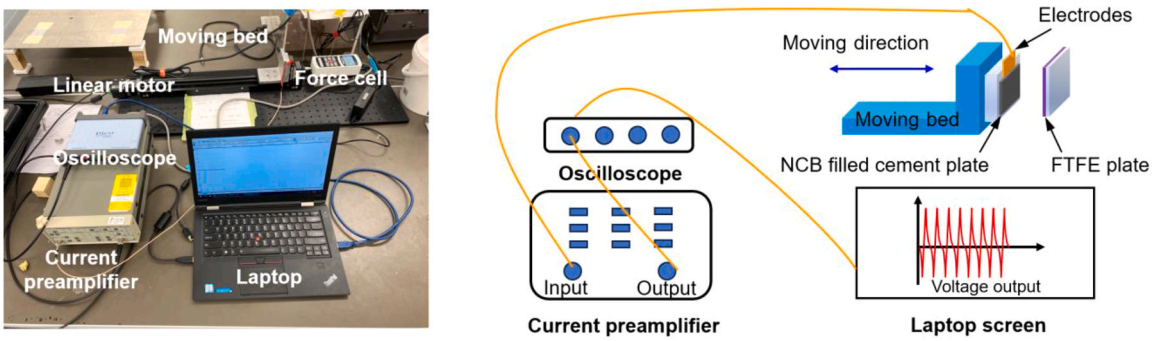

(a) Test setup illustration for triboelectric self-powering test

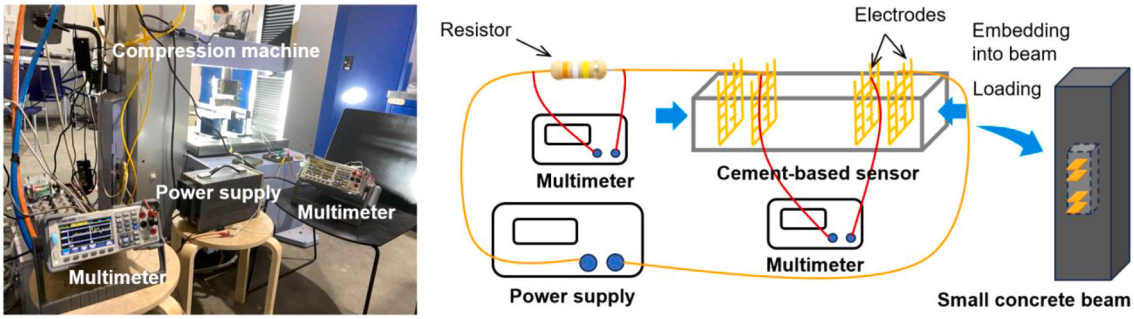

(b) Test setup for piezoresistive self-sensing test

Fig. 3. Experimental setup and schematic plot for the triboelectric self-powering and piezoresistive self-sensing tests.

performance is evaluated by applying uniaxial cyclic compression directly on the cement-based sensors, and then further explored on its self-sensing performance embedded into concrete beams. The effects of loading amplitude, loading rate, and holding period on the stability and reversibility of cement-based sensors are investigated.

3. Results and discussions

3.1. Triboelectric capability

As schematically illustrated in Fig. 4a, the working mechanism of CBTENG initially originates from contact electrification. When the PTFE plate contacts with the cement-based plate under pressure, electrons transfer from the cement plate to the PTFE plate because of the higher electron affinity of PTFE. This transfer results in the cement plate acquiring positive charges and the PTFE plate obtaining equal negative charges (Fig. 4a, ii). When the forces are released and the PTFE plate moves away from the cement-based plate, electrostatic induction starts to play the dominant role. In the positively charged cement-based plate, it attracts the electrons in the nickel foam electrode toward the cement-nickel foam interface, forming an electrical double layer (EDL) structure at the interfaces. Therefore, when the nickel foam is connected to the ground and establishes an open circuit, electrons can continuously flow from the ground to the nickel foam until the circuit reaches a neutral state (Fig. 4a, iv).

The repeated contact and separation of the PTFE plate and cement-based plate will generate a series of alternative currents (AC). Under the constant load of 10 N, the voltage was measured for the CBTENG with different surface areas at varying loading frequencies. Considering that civil engineering structures are typically subjected to low-frequency loads, the loading frequency was set between 1/2 Hz and 4 Hz. As displayed in Fig. 4b, the voltage of 10 × 10 × 5 mm cement-based TENG

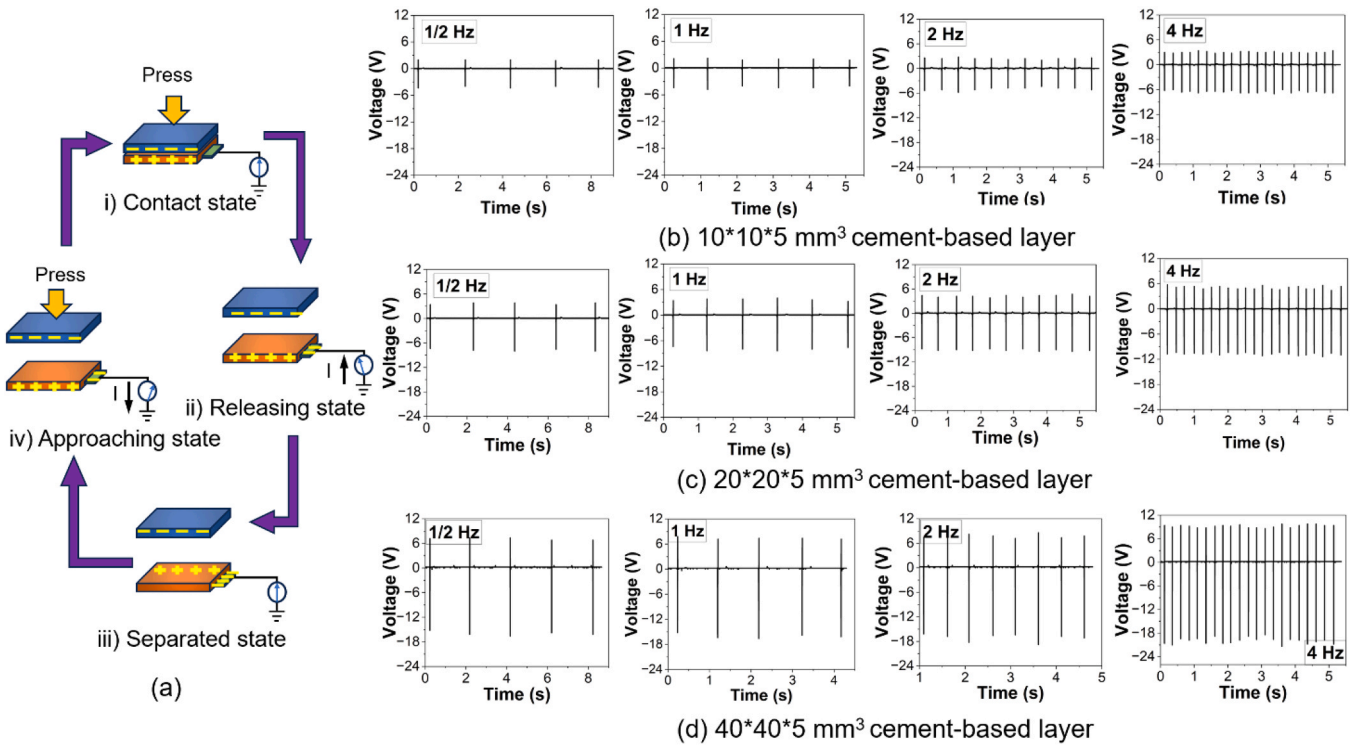

Fig. 4. Single-electrode mode of cement-based TENG and the output voltage: (a) schematic plot of triboelectric mechanism in the cement-based TENG; (b) voltage of $10 \times 10 \times 5$ mm^3 cement-based TENG under various load frequencies; (c) voltage of $20 \times 20 \times 5$ mm^3 cement-based TENG under various load frequencies; (d) voltage of $40 \times 40 \times 5$ mm^3 cement-based TENG under various load frequencies.

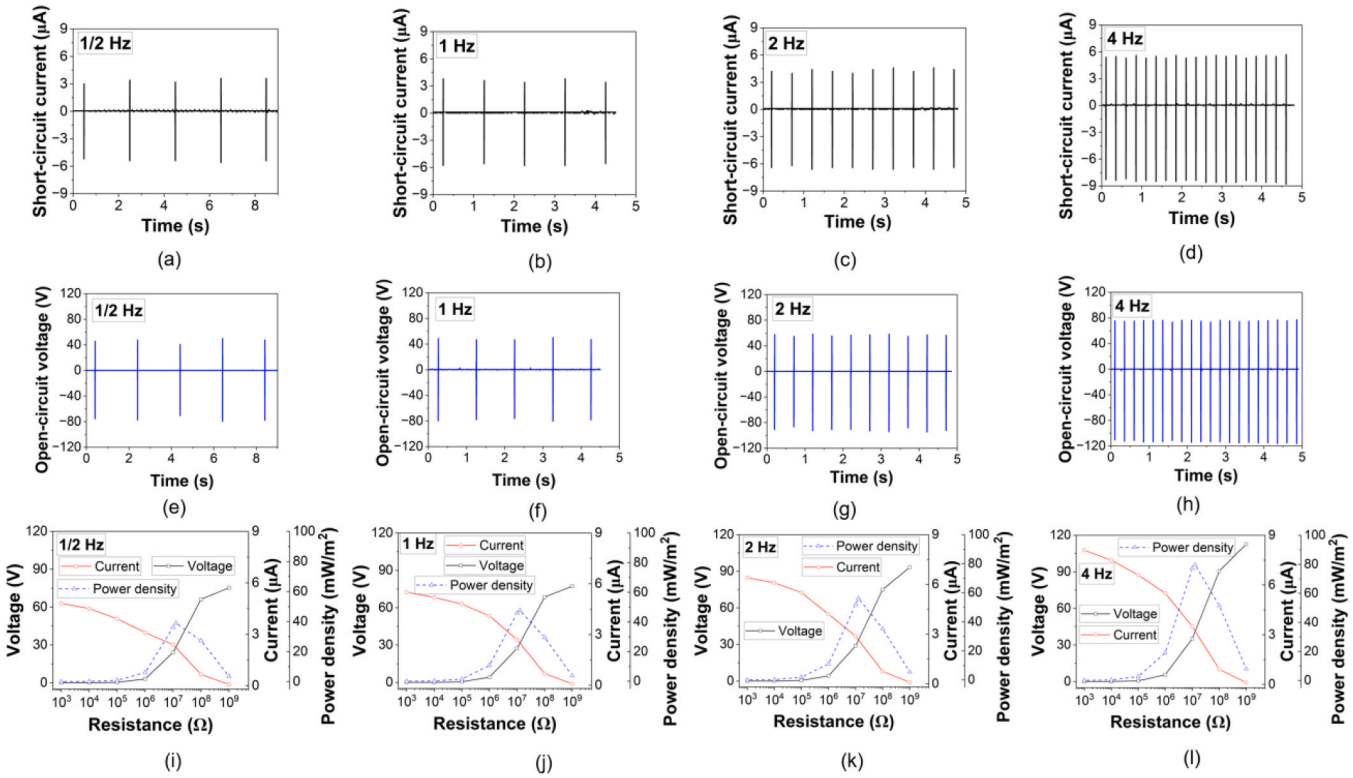

Fig. 5. Output short-circuits current and open-circuit voltage of $40 \times 40 \times 5$ mm^3 cement-based TENG under various load frequencies: (a) to (d) short-circuit currents at the loading frequencies of 1/2, 1, 2, and 4 Hz, respectively; (e) to (f) open-circuit voltages at the loading frequencies of 1/2, 1, 2, and 4 Hz, respectively; (i) to (l) voltage, current and power density outputs with various resistors at the loading frequencies of 1/2, 1, 2, and 4 Hz, respectively.

reached 6.7, 6.8, 8.4, and 9.2 V, respectively at the frequencies 1/2, 1, 2, and 4 Hz. The increase in loading frequency leads to a higher voltage because higher frequencies result in more frequent contact and separation cycles between the layers, which enhances the charge transfer and accumulation, thereby increasing the overall triboelectric voltage. The triboelectric performances of 20 × 20 × 5 mm and 40 × 40 × 5 mm cement-based TENGs are shown in Fig. 4c and Fig. 4d, respectively. The triboelectric voltage is higher than that of the smallest plate, reaching 11.8, 12.0, 13.5, and 16.7 V at the frequencies 1/2, 1, 2, and 4 Hz, respectively. The highest triboelectric voltages are generated for the largest cement-based plate with the values reaching 23.1, 23.3, 25.1, and 30.5 V at various frequencies. The finding indicates that the voltage increases with the surface area of the plates, but the changing mode is not linear. The former is easily understood, as larger surface areas provide more contact points, thereby increasing the amount of charge generated during each contact and separation process. In terms of non-linearity, there are several potential reasons. First, the cement matrix is inhomogeneous on a micro-scale with multiple phases such as calcium silicate hydrate (C-S-H), ettringite (AFt), calcium hydroxide (CH), etc. These materials have various electronegativity values and triboelectric capabilities. Second, the larger surface area increases the capacitance of the cement matrix. As capacitance increases, the voltage does not increase proportionally to the charge, leading to a non-linear relationship in voltage increase [37]. Third, the PTFE is usually flexible, but the cement-based plate is solid without remarkable deformation ability, hence, their contact quality is dependent on the smooth and surface conditions of the two plates. The detailed discussion will be displayed in Section 3.4.

The 40 × 40 × 5 mm^3 CBTENG with the highest voltage output is selected to investigate their short-circuit current and open-circuit voltage at various frequencies. Fig. 5 illustrates the output current and voltage under various load frequencies. The analysis is divided into two

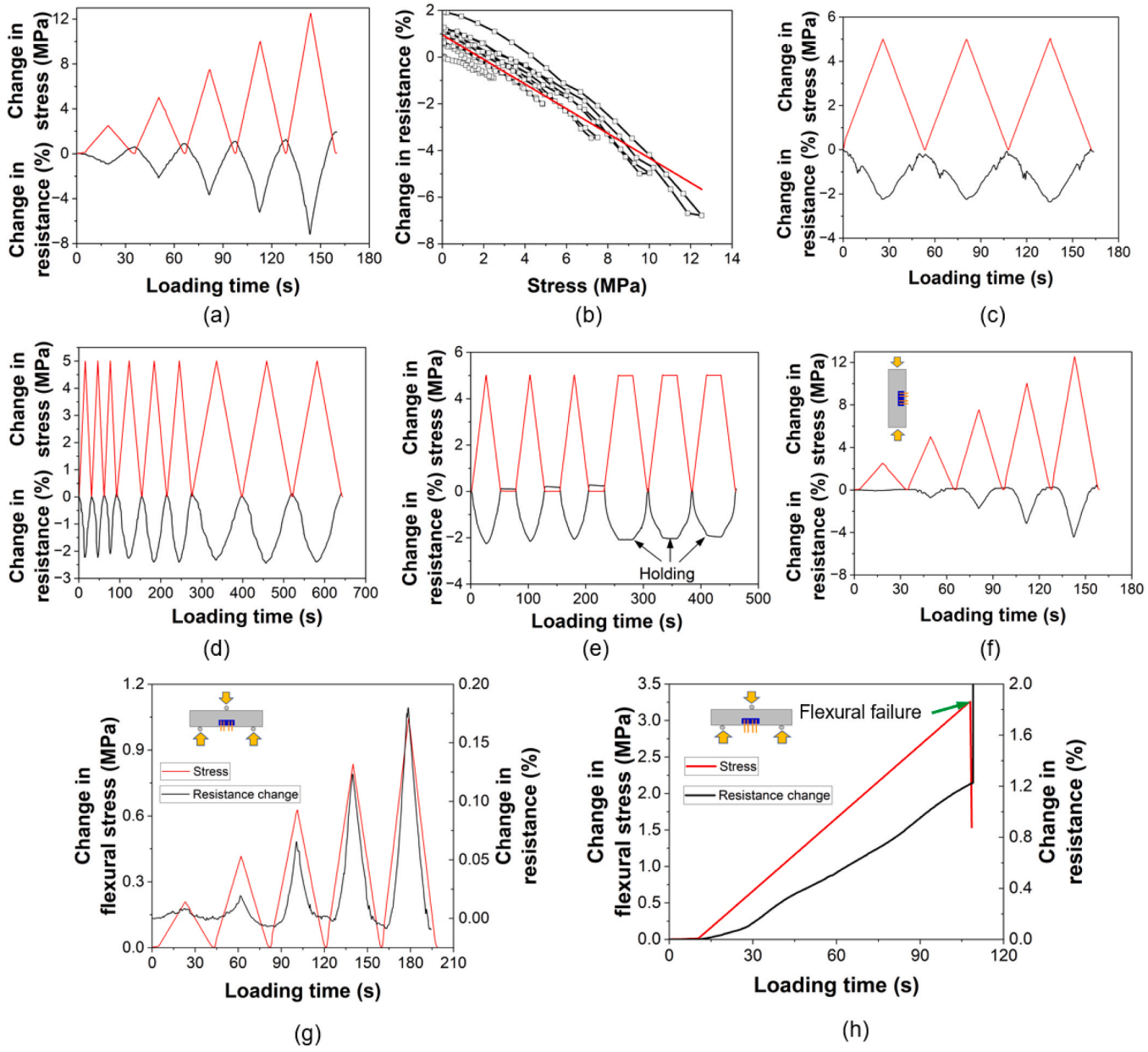

Fig. 6. Piezoresistive stress sensing performance of NCB filled cement-based sensor: (a) in different compressive stress magnitudes; (b) resistance to stress changes; (c) at three duplicated stress cycles; (d) in different loading rates; (e) holding without stress and holding at a constant stress of 5 MPa; (f) in different compressive stress magnitudes when embedded at a concrete beam; (g) in different flexural stress magnitudes when embedded at the tension zone; (h) flexural damage sensing performance.

main parts: short-circuit current and open-circuit voltage, both evaluated at loading frequencies of 1/2, 1, 2, and 4 Hz. The short-circuit current generated by the CBTENG at different frequencies is shown in Fig. 5a to d. As the frequency increases from 1/2 Hz to 4 Hz, the amplitude of the short-circuit current exhibits a noticeable increase from approximately 5.3 μA to 8.2 μA. This suggests that the current output is positively correlated with the loading frequency, which is consistent with the principles of triboelectric energy generation where higher frequencies induce more frequent contact-separation cycles, leading to increased charge transfer and thus higher current output [38,39]. Fig. 5e to h display the open-circuit voltage output at the same loading frequencies. Similar to the short-circuit current, the voltage output also increases with frequency. At 1/2 Hz, the average voltage peak is around 78 V, which gradually increases with frequency to nearly 113 V. The observed increase in open-circuit voltage with frequency can be attributed to the enhanced triboelectric effect at higher frequencies, where more rapid motion results in more frequent contact and separation between the triboelectric layers, thereby generating higher voltages [40,41]. In terms of the power density of CBTENG, it is determined by recording the output voltage and current of the CBTENG, which is connected to a series of resistors with values of 1 kΩ, 10 kΩ, 100 kΩ, 1 MΩ, 10 MΩ, 100 MΩ, and 1 GΩ. Fig. 5i to l exhibit the voltage, current, and power density at the loading frequencies of 1/2, 1, 2, and 4 Hz, respectively. Across all frequencies, the output voltage increases and current decreases with higher resistance, and the power density curves display a clear peak at an intermediate resistance value, indicating an optimal energy transfer with a specific resistance. Especially, the highest power density increases from 39 to 83 mW/m^2 as the loading frequency increases from 1/2–4 Hz.

3.2. Piezoresistive self-sensing capability

Fig. 6 presents the piezoresistive self-sensing cement-based sensors in various scenarios including different loading magnitudes, loading rates, stability, repeatability, and whether embedded inside the concrete beam or not. In Fig. 6a, the cement-based sensor exhibits a clear piezoresistive effect, where the change of electrical resistance correlates well with the applied compressive stress. The resistance of the cement matrix decreases as the stress increases. This is because the NCB particles in the cement matrix are compressed under compressive stress, causing them to move closer to each other. The black curve representing resistance change closely follows the red stress curve reaching nearly 7.5 % when the stress reaches 12.5 MPa, indicating that the cement-based sensor reliably responds to different levels of compressive stress. Fig. 6b illustrates the relationship between resistance changes and applied stress, demonstrating an almost linear correlation between resistance variation and compressive stress. This suggests the sensor's potential for detecting varying levels of compressive stress in real-time applications. Fig. 6c demonstrates the sensor's performance over three duplicated stress cycles of 5 MPa, which is within the elastic range of cementitious composite. The cement-based sensor maintains a consistent response, evidenced by the repetition of the resistance change across stress cycles. This consistency highlights the reliability and repeatability of the cement-based sensor's performance, which is crucial for practical applications requiring sustained monitoring. Fig. 6d shows the sensing performance under three varying loading rates. The resistance change shows a strong correlation with the stress curve across different loading durations. It demonstrates that self-sensing performance is independent of the loading rate, which indicates its robustness and adaptability to different dynamic conditions. Fig. 6e explores the cement-based sensor's behavior during a holding phase with no stress applied while maintaining a constant stress of 5 MPa. Resistance remains stable during the holding period without stress, and the response under constant stress further validates the sensor's stability and accuracy under steady-state conditions.

Fig. 6f shows the cement-based sensor's performance when embedded in a concrete beam under different compressive stress magnitudes. Although the force is applied to the concrete beam rather than directly to the cement-based sensor, the stress transfer causes the embedded cement-based sensor to experience compressive stress, thereby reducing its electrical resistance. The change of resistance closely mirrors the stress variations, confirming the sensor's effectiveness even when integrated into structural components. This demonstrates its potential application in SHM, where real-time stress detection within concrete structures is critical. However, it is noteworthy that the change in resistance is smaller than that subjected to direct load, indicating a reduction in the force acting on the cement-based sensor. This reduction can be attributed not only to the surrounding cement matrix bearing part of the load but also to the load transfer and the interface between the sensor and the cement matrix, both of which affect the sensor's sensitivity. Fig. 6g investigates the cement-based sensor's response to different flexural stress magnitudes at a three-point bending test when embedded in the tension zone of a concrete beam. The sensor effectively captures the variations in flexural stress, as indicated by the close alignment between the resistance change and flexural stress curves. It suggests that the cement-based sensor can be used for monitoring the flexural stress of concrete beams. Considering that concrete beams are most susceptible to bending failure, Fig. 6h assesses the cement-based sensor's behavior in detecting flexural damage. The gradual increase in both stress and resistance changes as loading time suggests that the sensor can monitor the onset and progression of damage. The increase of resistance is mainly due to the generation of micro cracks. As the concrete beam reaches the failure, the resistance value suddenly increases, which is caused by the generation of main cracks and the disruption of the conductive pathways within the cement-based sensor [42,43]. The linear correlation between stress and resistance further emphasizes the sensor's potential for early damage detection, which is vital for preventive maintenance in structural applications.

3.3. Mechanical, micro and charging properties

The mechanical properties of cement-based materials are crucial for their safe application in pavements and structures. Fig. 7a depicts the stress-strain curve of cubic cement-based materials under uniaxial compression, showing a high compressive strength exceeding 50 MPa and elastic modulus around 20 GPa, which meets the requirements for most applications. Due to its unique characteristics of heat release during hydration, cement-based materials often develop various sizes of voids both on their surface and internally. This can be evidenced by the SEM images regarding the surface of the cement-based layer as depicted in Fig. 7b. Previous studies have indicated that surficial porosity can increase the effective surface area of TENG, rendering the surface rougher and facilitating charge separation [44]. Hence, the surficial microstructures of cement-based triboelectric layer provide a favorable factor for the development of the CBTENG. Fig. 7c illustrates the equivalent circuit for charging a commercial 10 μF capacitor using a CBTENG. Since the generator produced AC, a rectifier was employed to convert the output AC into DC.

The charging rate of $40 \times 40 \times 5$ mm^3 CBTENG at various load frequencies is displayed in Fig. 7d. It shows that the CBTENG can charge up a 10 μF capacitor to 0.32 V in approximately 250 s at the load frequency of 1 Hz. As the frequency increases to 2 Hz, the charging time rapidly decreases to approximately one-fifth of the original, reaching nearly 48 s. With further increases in frequency to 3 Hz and 4 Hz, the charging time continues to decrease, but the reduction is much less significant than before. The fastest charging rate occurs at the frequency of 4 Hz in around 25 s. For the $20 \times 20 \times 5$ mm^3 CBTENG, the charging time is nearly 300 s to reach 0.32 V. The other trends remain consistent with previous observations: as the frequency increases, the charging time decreases. However, the rate of reduction slows as the frequency rises to 4 Hz (Fig. 7e). It is worth noting that only the results at the

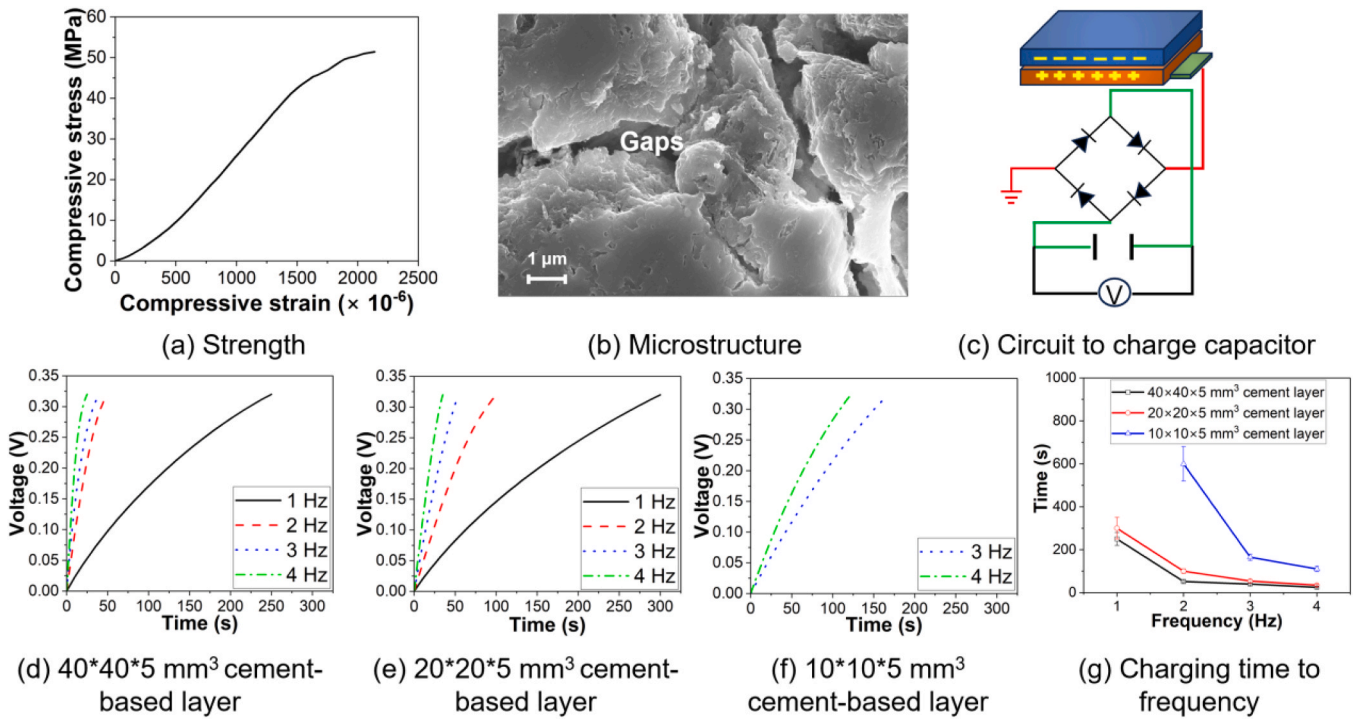

Fig. 7. Mechanical, microstructural and charging performances of cement-based TENG: (a) compressive stress-strain curve of cubic cement matrix; (b) micro-morphology on the surface of cement-based plate; (c) circuit to charge capacitor by cement-based TENG; (d) to (f) charging rate of the cement-based TENG with surface areas of 10 × 10, 20 × 20 and 40 × 40 mm^2 under various frequencies; (g) charging time to frequency.

frequencies of 3 Hz and 4 Hz are plotted for the 10 × 10 × 5 mm^3 CBTENG, due to the low frequency 1 Hz and 2 Hz never rise the voltage to the specific value (Fig. 7f). At low frequencies, the time interval between each cycle is longer, allowing more time for charges to leak or dissipate through various pathways, such as environmental humidity, leakage paths within the material, or resistance at the contact interface [45]. Additionally, at low frequencies, surface charges have more time to redistribute and return to equilibrium, which prevents charge accumulation and voltage growth [46]. Fig. 7g shows the relationship between charging time and load frequency. To charge up the 10 μF capacitor to 0.32 V, the 10 × 10 × 5 mm^3 CBTENG struggles to charge the capacitor to the specified voltage at low frequencies. At the

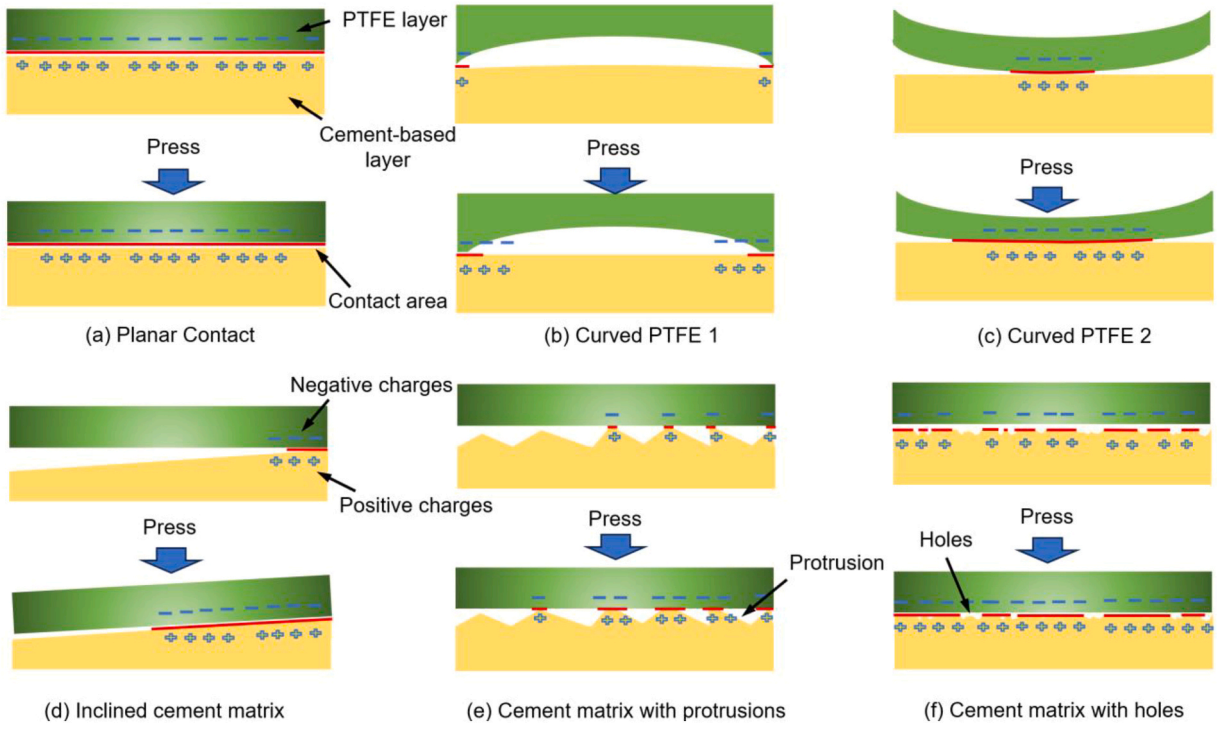

Fig. 8. Various contact states between PTFE and cement-based triboelectric layers.

frequency of 1 Hz, it takes over 600 s to reach 0.32 V. The $20 \times 20 \times 5$ mm^3 and $40 \times 40 \times 5$ mm^3 CBTENGs can charge much faster, and there is no significant difference in their charging times especially at the high frequency.

3.4. Mechanism discussion

3.4.1. Triboelectric self-powering capability

The experimental results indicate that the power generation efficiency of CBTENG does not increase proportionally with surface area. Given that the dimensions of civil engineering structures typically range from a few centimeters to meters and kilometers, it is meaningful to investigate the optimal size of cement-based triboelectric nanogenerators for future practical applications. The contact state between the PTFE and cement-based triboelectric layers is the first foundational factor that should be addressed. Fig. 8a to f illustrate all the potential contact states in the CBTENG. From a macroscopic perspective, it can be assumed that the two plates are in complete contact (Fig. 8a). However, at the microscopic level, the contact between the cement-based and PTFE plates is highly dependent on the surface condition of the cement matrix and the smoothness of the PTFE plate, hence, their contact can be considered as the integration of all those situations in Fig. 8.

Due to its low stiffness, PTFE plates are prone to bending, especially under long-term cyclic loading, which inevitably affects their curvature. In contrast, cementitious materials, characterized by higher stiffness and strength, are unlikely to undergo permanent deformation under pressure. Therefore, their relative contact states can be exhibited in Fig. 8b and c. In the case of the cement-based triboelectric layer, inclined surfaces are present whether during the casting or cutting processes in Fig. 8d. The inclination alters the contact pattern between the two surfaces, reducing the contact area and resulting in uneven contact. This can cause an uneven distribution of triboelectric charges, thereby affecting the efficiency of power generation. Moreover, the surface of the cement-based layer is not completely smooth, particularly in the presence of aggregate. Hence, small protrusions or holes may occur due to the prominence of the aggregate or its detachment (Fig. 8e and f). The surficial protrusions can increase the number of contact points, potentially enhancing the output voltage and current of the CBTENG. However, excessively large protrusions may reduce the contact area in the surrounding regions and intensify the mechanical wear of the TENG device. Conversely, the surficial holes decrease the contact area, leading to a more concentrated charge distribution, which is detrimental to the overall charge transfer efficiency.

This study does not address the effects of varying pressures on the triboelectric efficiency of CBTENGs. However, it is evident that higher pressure increases the effective contact area between the two layers, thereby enhancing the rate of charge generation. In terms of the size of CBTENG, larger surfaces are more likely to have the abovementioned defects, protrusions, holes, and are more prone to bending. Conversely, contact points on smaller scales tend to fit more precisely. This explains why cement-based triboelectric nanogenerators with sizes of 20 cm and 40 cm exhibit similar charging speeds for a 10 μF capacitor under relatively high-frequency conditions.

3.4.2. Piezoresistive self-sensing capability

Fig. 9 illustrates the conductive and piezoresistive mechanisms of NCB filled cement-based sensors under various loading conditions. Initially, the cement-based sensor is in its intact state with uniformly distributed NCB particles (Fig. 9a). At this stage, the NCB particles are not influenced by external load, which means there is no significant change in the conductive pathways within the cement matrix. When the cement-based sensor is subjected to compression, the NCB particles get closer to each other, leading to the formation of new conductive pathways (depicted by red dashed lines in Fig. 9b). The well-maintained electrical resistance in the holding period demonstrates the stable contact between NCB particles. The approached NCB particles enhance the sensor's electrical conductivity due to the improved contact between NCB particles, which contributes to the piezoresistive effect. As the particles approach each other, the resistance decreases, which can be detected and measured as a response to the compressive load. On the contrary, the conductive pathways are disrupted, leading to an increase in electrical resistance under tensile stress, where the NCB particles within the cement matrix begin to separate (Fig. 9c). During a three-point bending test, the cement-based sensor experiences both compression and tension simultaneously (Fig. 9d). In the compression zone, the NCB particles approach each other, similar to the behavior in Fig. 9b, forming new conductive pathways. Conversely, in the tension zone, the NCB particles move apart, leading to disrupted conductive pathways. This dual behavior creates a complex piezoresistive response, with varying resistance depending on the location within the sensor [47]. In other word, the resistance decreases in the compression zone, while it increases in the tension zone. The overall resistance output is the sum of these two effects. Overall, it demonstrates the cement-based sensor's sensitivity to different types of mechanical loads, with distinct conductive and piezoresistive mechanisms depending on whether the sensor is in compression, tension, or bending. The movement of NCB particles in response to external forces is the key factor in altering the electrical properties of the cement-based sensor, making it a valuable

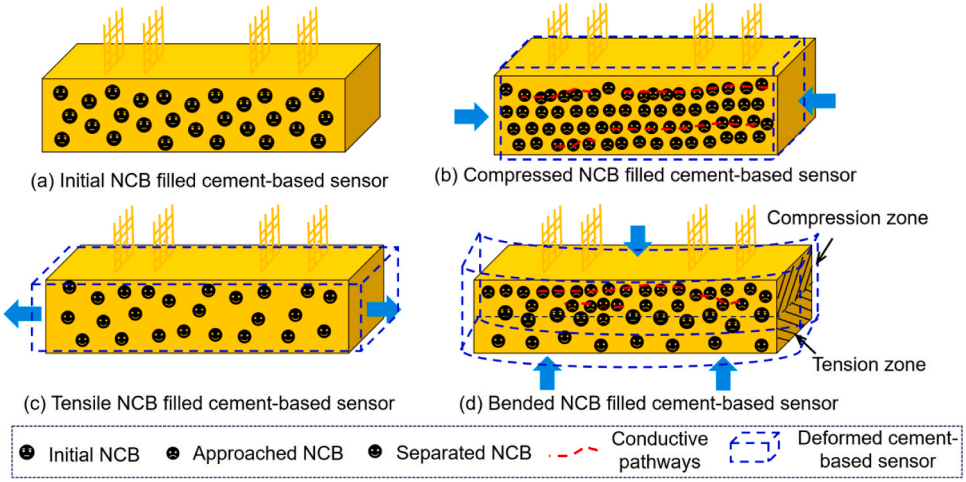

Fig. 9. Conductive and piezoresistive mechanism of NCB filled cement-based sensors in various loading conditions: (a) the intact cement-based sensor; (b) the compressed cement-based sensor; (c) the cement-based sensor in tension; (d) the cement-based sensor in three-point bending test.

alternative for SHP and other applications.

4. Conclusions

This study first developed the triboelectric self-powering and piezoresistive self-sensing cement-based sensors based on the NCB filled cementitious materials. The triboelectric test was conducted on the fully cured NCB reinforced thin cement plate and PTFE plate. The piezoresistive test was carried out on the individual cement-based sensor with embedded electrodes and concrete beams with embedded cement-based sensors. Some key conclusions are listed below:

(1) The triboelectric properties of fully cured cement substrates closely mimic their civil engineering applications, promoting the potential use of CBTENG in pavements and structures. The voltage output firmly relates to the loading frequency, showing an increasing tendency with the increase of frequency. At a frequency of 4 Hz, the $40 \times 40 \times 5$ mm^3 CBTENG can generate a peak AC voltage of up to 30.5 V.
(2) The short-circuit current and open-circuit voltage of $40 \times 40 \times 5$ mm^3 CBTENG can reach up to 8.2 μA and 113 V at the frequency of 4 Hz, which is able to recharge a 10 μF capacitor to 0.32 V within 25 seconds after being rectified to DC. The compressive strength and microstructures of NCB filled cementitious composites also exhibit satisfactory mechanical and NCB dispersion properties.
(3) In terms of piezoresistivity, the NCB filled cement-based sensor demonstrates consistent and reliable piezoresistive responses across various loading conditions. Its ability to detect both compressive and tensile stresses, as well as its performance in structural elements like concrete beams, highlights its potential for real-world applications in structural health monitoring and damage detection.
(4) The findings also demonstrated that larger specimens exhibit a lower percentage of effective contact area due to the uneven surfaces of both the cement-based and PTFE plates, as well as the small protrusions and holes on the cement-based surface. Therefore, it is necessary to further investigate the specific dimensions of CBTENG to maximize power generation while ensuring minimal impact on their mechanical, durable and other properties.
(5) The movement of NCB particles and their relative location depend on their loading conditions and the embedding location inside a structural element. Under compression, these particles move closer together, while under tension, they move apart, causing corresponding increases and decreases in electrical resistance.

CRediT authorship contribution statement

Wengui Li: Writing – review & editing, Writing – original draft, Validation, Supervision, Resources, Conceptualization. **Fan Wu:** Writing – review & editing, Writing – original draft, Validation. **Long Shi:** Writing – review & editing, Writing – original draft, Validation. **Yunan Huang:** Writing – review & editing, Writing – original draft, Validation. **Kejin Wang:** Writing – review & editing, Writing – original draft, Validation, Supervision. **Shuhua Peng:** Writing – review & editing, Writing – original draft, Validation, Supervision, Resources. **Wenkui Dong:** Writing – review & editing, Writing – original draft, Validation, Methodology, Investigation, Formal analysis.

Declaration of Competing Interest

The authors declare that they have no known competing financial interests or personal relationships that could have appeared to influence the work reported in this paper.

Acknowledgements

The authors would like to acknowledge the support from Australian Research Council (ARC), Australia (FT220100177, LP230100288, DP220101051, DP220100036, IH200100010).

Data availability

Data will be made available on request.

References

[1] W. Dong, W. Li, Z. Tao, K. Wang, Piezoresistive properties of cement-based sensors: review and perspective, Constr. Build. Mater. 203 (2019) 146–163.
[2] W. Li, F. Qu, W. Dong, G. Mishra, S.P. Shah, A comprehensive review on self-sensing graphene/cementitious composites: a pathway toward next-generation smart concrete, Constr. Build. Mater. 331 (2022) 127284.
[3] W. Li, W. Dong, Y. Guo, K. Wang, S.P. Shah, Advances in multifunctional cementitious composites with conductive carbon nanomaterials for smart infrastructure, Cem. Concr. Compos. 128 (2022) 104454.
[4] B. Han, S. Ding, X. Yu, Intrinsic self-sensing concrete and structures: a review, Measurement 59 (2015) 110–128.
[5] D.D.L. Chung, A critical review of electrical-resistance-based self-sensing in conductive cement-based materials, Carbon 203 (2023) 311–325.
[6] Y. Guo, W. Li, W. Dong, Z. Luo, F. Qu, F. Yang, K. Wang, Self-sensing performance of cement-based sensor with carbon black and polypropylene fibre subjected to different loading conditions, J. Build. Eng. 59 (2022) 105003.
[7] L. Chen, M. Ren, J. Zhou, X. Zhou, F. Liu, J. Di, P. Xue, C. Li, Q. Li, Y. Li, L. Wei, Q. Zhang, Bioinspired iontronic synapse fibers for ultralow-power multiplexing neuromorphic sensorimotor textiles, Proc. Natl. Acad. Sci. 121 (33) (2024) e2407971121.
[8] Y. Li, Z. Qiu, H. Kan, Y. Yang, J. Liu, Z. Liu, W. Yue, G. Du, C. Wang, N.-Y. Kim, A human-computer interaction strategy for an FPGA platform boosted integrated "Perception-Memory" system based on electronic tattoos and memristors, Adv. Sci. 11 (39) (2024) 2402582.
[9] J. Zhang, H. Wang, P. Blanloeuil, G. Li, Z. Sha, D. Wang, W. Lei, C. Boyer, Y. Yu, R. Tian, C.H. Wang, Enhancing the triboelectricity of stretchable electrospun piezoelectric polyvinylidene fluoride/boron nitride nanosheets composite nanofibers, Compos. Commun. 22 (2020) 100535.
[10] Y. Qiao, W. Chang, A.J. Cheng, J. Wang, H. Zhang, Z. Sha, S. He, J. Zhang, S. Peng, C.H. Wang, Clapping triboelectric nanogenerators as self-powered, frequency-insensitive and gravity-independent vibration sensors, Nano Energy 118 (2023) 109021.
[11] G. Li, S. Wu, Z. Sha, L. Zhao, D. Chu, C.H. Wang, S. Peng, A triboelectric nanogenerator powered piezoresistive strain sensing technique insensitive to output variations, Nano Energy 108 (2023) 108185.
[12] Q. Tang, Z. Wang, W. Chang, J. Sun, W. He, Q. Zeng, H. Guo, C. Hu, Interface static friction enabled ultra-durable and high output sliding mode triboelectric nanogenerator, Adv. Funct. Mater. 32 (26) (2022) 2202055.
[13] F. Azhari, N. Banthia, Cement-based sensors with carbon fibers and carbon nanotubes for piezoresistive sensing, Cem. Concr. Compos. 34 (7) (2012) 866–873.
[14] D. A, S. D, M. Pichumani, Electro-mechanical investigations of steel fiber reinforced self-sensing cement composite and their implications for real-time structural health monitoring, J. Build. Eng. 51 (2022) 104343.
[15] S.H. Lee, S. Kim, D.-Y. Yoo, Hybrid effects of steel fiber and carbon nanotube on self-sensing capability of ultra-high-performance concrete, Constr. Build. Mater. 185 (2018) 530–544.
[16] Z. Deng, A.H. Mahmood, W. Dong, D. Sheng, X. Lin, W. Li, Piezoresistive performance of self-sensing bitumen emulsion-cement mortar with multi-walled carbon nanotubes, Cem. Concr. Compos. 153 (2024) 105718.
[17] W. Dong, W. Li, K. Wang, S.P. Shah, Physicochemical and Piezoresistive properties of smart cementitious composites with graphene nanoplates and graphite plates, Constr. Build. Mater. 286 (2021) 122943.
[18] W. Dong, W. Li, X. Zhu, D. Sheng, S.P. Shah, Multifunctional cementitious composites with integrated self-sensing and hydrophobic capacities toward smart structural health monitoring, Cem. Concr. Compos. 118 (2021) 103962.
[19] A. D'Alessandro, M. Tiecco, A. Meoni, F. Ubertini, Improved strain sensing properties of cement-based sensors through enhanced carbon nanotube dispersion, Cem. Concr. Compos. 115 (2021) 103842.
[20] G.H. Nalon, J.C.L. Ribeiro, E.N.Dd Araújo, L.G. Pedroti, J.M.Fd Carvalho, R. F. Santos, A. Aparecido-Ferreira, Effects of different kinds of carbon black nanoparticles on the piezoresistive and mechanical properties of cement-based composites, J. Build. Eng. 32 (2020) 101724.
[21] W. Dong, W. Li, N. Lu, F. Qu, K. Vessalas, D. Sheng, Piezoresistive behaviours of cement-based sensor with carbon black subjected to various temperature and water content, Compos. Part B Eng. 178 (2019) 107488.
[22] F.-R. Fan, Z.-Q. Tian, Z. Lin Wang, Flexible triboelectric generator, Nano Energy 1 (2) (2012) 328–334.
[23] F.-R. Fan, L. Lin, G. Zhu, W. Wu, R. Zhang, Z.L. Wang, Transparent triboelectric nanogenerators and self-powered pressure sensors based on micropatterned plastic films, Nano Lett. 12 (6) (2012) 3109–3114.

[24] Y. Li, Q. Lin, T. Sun, M. Qin, W. Yue, S. Gao, A perceptual and interactive integration strategy toward telemedicine healthcare based on electroluminescent display and triboelectric sensing 3D stacked device, Adv. Funct. Mater. 34 (40) (2024) 2402356.
[25] Z.-H. Lin, Y. Xie, Y. Yang, S. Wang, G. Zhu, Z.L. Wang, Enhanced triboelectric nanogenerators and triboelectric nanosensor using chemically modified TiO2 nanomaterials, ACS Nano 7 (5) (2013) 4554–4560.
[26] N. Jayababu, D. Kim, ZnO nanorods@conductive carbon black nanocomposite based flexible integrated system for energy conversion and storage through triboelectric nanogenerator and supercapacitor, Nano Energy 82 (2021) 105726.
[27] J. Sintusiri, V. Harnchana, V. Amornkitbamrung, A. Wongsa, P. Chindaprasirt, Portland Cement-TiO2 triboelectric nanogenerator for robust large-scale mechanical energy harvesting and instantaneous motion sensor applications, Nano Energy 74 (2020) 104802.
[28] W. Dong, W. Li, K. Wang, Z. Luo, D. Sheng, Self-sensing capabilities of cement-based sensor with layer-distributed conductive rubber fibres, Sens. Actuators A Phys. 301 (2020) 111763.
[29] W. Dong, W. Li, L. Shen, D. Sheng, Piezoresistive behaviours of carbon black cement-based sensors with layer-distributed conductive rubber fibres, Mater. Des. 182 (2019) 108012.
[30] N. Phromviyo, J. Boonlakhorn, P. Posi, P. Thongbai, P. Chindaprasirt, Dielectric and mechanical properties of CTAB-modified natural rubber latex–cement composites, Polymers (2022).
[31] W. Thongthapthai, V. Harnchana, C. Chanthad, V. Amornkitbamrung, P. Chindaprasirt, The fabrication of calcium silicate-natural rubber composite for mechanical energy harvesting, Surf. Interfaces 25 (2021) 101180.
[32] S. Kuntharin, V. Harnchana, J. Sintusiri, P. Thongbai, A. Klamchuen, K. Sinthiptharakoon, V. Amornkitbamrung, P. Chindaprasirt, Smart triboelectric floor based on calcium silicate-carbon composite for energy harvesting and motion sensing applications, Sens. Actuators A Phys. 358 (2023) 114423.
[33] W. Dong, S. Gao, S. Peng, L. Shi, S.P. Shah, W. Li, Graphene reinforced cement-based triboelectric nanogenerator for efficient energy harvesting in civil infrastructure, Nano Energy 131 (2024) 110380.
[34] W. Dong, W. Li, K. Wang, S.P. Shah, D. Sheng, Multifunctional cementitious composites with integrated self-sensing and self-healing capacities using carbon black and slaked lime, Ceram. Int. 48 (14) (2022) 19851–19863.
[35] W. Dong, W. Li, G. Long, Z. Tao, J. Li, K. Wang, Electrical resistivity and mechanical properties of cementitious composite incorporating conductive rubber fibres, Smart Mater. Struct. 28 (8) (2019) 085013.
[36] W. Dong, W. Li, Y. Guo, X. He, D. Sheng, Effects of silica fume on physicochemical properties and piezoresistivity of intelligent carbon black-cementitious composites, Constr. Build. Mater. 259 (2020) 120399.
[37] S. Zargari, A. Rezania, Z.D. Koozehkanani, H. Veladi, J. Sobhi, L. Rosendahl, Effect of the inherent capacitance optimization on the output performance of triboelectric nanogenerators, Nano Energy 92 (2022) 106740.
[38] T. Cheng, J. Shao, Z.L. Wang, Triboelectric nanogenerators, Nat. Rev. Methods Prim. 3 (1) (2023) 39.
[39] J. Shao, M. Willatzen, T. Jiang, W. Tang, X. Chen, J. Wang, Z.L. Wang, Quantifying the power output and structural figure-of-merits of triboelectric nanogenerators in a charging system starting from the Maxwell's displacement current, Nano Energy 59 (2019) 380–389.
[40] A.A. Maamoun, A.A. Mahmoud, D.M. Naeim, M. Arafa, A.M. Esawi, Effect of density and thickness of flexible polyurethane foam on the performance of triboelectric nanogenerators, Mater. Adv. (2024).
[41] C. Shan, K. Li, Y. Cheng, C. Hu, Harvesting environment mechanical energy by direct current triboelectric nanogenerators, Nano-Micro Lett. 15 (1) (2023) 127.
[42] W. Dong, W. Li, Z. Luo, G. Long, K. Vessalas, D. Sheng, Structural response monitoring of concrete beam under flexural loading using smart carbon black/cement-based sensors, Smart Mater. Struct. 29 (6) (2020) 065001.
[43] F. Naeem, H.K. Lee, H.K. Kim, I.W. Nam, Flexural stress and crack sensing capabilities of MWNT/cement composites, Compos. Struct. 175 (2017) 86–100.
[44] M.N. Biutty, S.I. Yoo, Enhanced performance of triboelectric nanogenerator by controlled pore size in polydimethylsiloxane composites with Au nanoparticles, Macromol. Res. 29 (1) (2021) 98–104.
[45] C. Liu, N. Zhang, J. Li, L. Dong, T. Wang, Z. Wang, G. Wang, X. Zhou, J. Zhang, Harvesting ultralow frequency (< 1 Hz) mechanical energy using triboelectric nanogenerator, Nano Energy 65 (2019) 104011.
[46] S. Niu, Z.L. Wang, Theoretical systems of triboelectric nanogenerators, Nano Energy 14 (2015) 161–192.
[47] F. Ubertini, A.L. Materazzi, A. D'Alessandro, S. Laflamme, Natural frequencies identification of a reinforced concrete beam using carbon nanotube cement-based sensors, Eng. Struct. 60 (2014) 265–275.
[48] W. Dong, J. Tang, K. Wang, Y. Huang, S.P. Shah, W. Li, Cement-based batteries for renewable and sustainable energy storage toward an energy-efficient future, Energy 315 (2025) 134382.
[49] W. Li, W. Dong, S.P. Shah. Multifunctional Cement-Based Sensors for Intelligent Infrastructure: Design, Fabrication and Application, CRC Press, 2024.
[50] X. Wang, Y. Guo, Z. Tao, L. Shi, W. Li, Self-heating performance of phase change cementitious mortar with hybrid carbon-based nanomaterials, J. Energy Storage 104 (2024) 114495.
[51] X. Wang, Y. Huang, L. Shi, S. Zhang, W. Li, Enhanced thermal performance of phase change mortar using multi-scale carbon-based materials, J. Build. Eng. 98 (2024) 111259.